# Electron scattering rate in epitaxial $YBa_2Cu_3O_7$ superconducting films

M. I. Flik, Z. M. Zhang, and K. E. Goodson
*Department of Mechanical Engineering, Massachusetts Institute of Technology, Cambridge, Massachusetts 02139*

M. P. Siegal and Julia M. Phillips
*AT&T Bell Laboratories, Murray Hill, New Jersey 07974*
(Received 25 October 1991; revised manuscript received 20 April 1992)

This work determines the electron scattering rate in the *a*-*b* plane of epitaxial $YBa_2Cu_3O_7$ films using two techniques. Infrared spectroscopy yields the scattering rate at temperatures of 10, 78, and 300 K by fitting reflectance data using thin-film optics and a model for the free-carrier conductivity. The scattering rate is also obtained using kinetic theory and an extrapolation of normal-state electrical resistivity data to superconducting temperatures based on the Bloch theory for the phonon-limited electrical resistivity of metals. The scattering rates determined using both techniques are in agreement and show that the electron mean free path in the *a*-*b* plane of $YBa_2Cu_3O_7$ superconducting films is three to four times the coherence length. Hence $YBa_2Cu_3O_7$ is pure but not in the extreme pure limit. An average defect interaction range of 4 nm is obtained using the defect density resulting from flux-pinning considerations.

## I. INTRODUCTION

The electron scattering rate is a basic parameter in theories for thermal and electrical transport properties and the optical behavior of metallic materials. At high temperatures scattering by phonons dominates the electron scattering processes. At low temperatures, electrons are scattered most frequently by lattice defects, and the electron scattering rate provides information about the defect structure of the material. In films of thickness comparable to the electron mean free path, the electron scattering rate is increased by boundary scattering. Below the critical temperature of a superconductor, the normal-state electrons possess a finite scattering rate, which affects the optical and thermal behavior of the superconductor. The determination of the electron scattering rate in $YBa_2Cu_3O_7$ has been made particularly important by the work of Hylton and Beasley,[1] who postulated a spacing between defects of 5.3 nm in the *a*-*b* plane of $YBa_2Cu_3O_7$ thin films from critical current density considerations. Using kinetic theory, the electron scattering rate and the spacing between defects yield an estimate of the interaction range of defects.

Kamaras *et al.*[2] performed an infrared spectroscopic study of the electron scattering rate of $YBa_2Cu_3O_7$ thin films. They used the Drude model and their results apply only to temperatures above the critical temperature. Goodson and Flik[3] predicted the electron mean free path and the electron scattering rate for *a*-*b* plane thermal conduction along epitaxial $YBa_2Cu_3O_7$ films in the superconducting state based on the single-crystal thermal conductivity and electrical resistivity data of Cohn *et al.*[4] Orenstein *et al.*[5] reviewed the infrared properties of $YBa_2Cu_3O_{7-\delta}$ crystals and discussed the residual scattering rate, due to electron scattering on impurities and defects, and the temperature-dependent scattering rate due to the interaction of electrons with phonons. But they did not obtain the electron scattering rate in the superconducting state from their spectroscopic study. By fitting microwave absorption data measured at 2 K for epitaxial $YBa_2Cu_3O_7$ films with a homogeneous two-fluid model, Miller *et al.*[6] obtained an average scattering rate of about 400 $cm^{-1}$ for film thicknesses from 400 to 500 nm. This is a surprising result because 400 $cm^{-1}$ is close to the scattering rate obtained at 300 K by Kamaras *et al.*,[2] Orenstein *et al.*,[5] and Zhang *et al.*[7] for $YBa_2Cu_3O_7$ films and crystals.

This work determines the electron scattering rate in the normal and superconducting states for $YBa_2Cu_3O_7$ films of varying thickness using infrared spectroscopy and electrical resistivity data. The samples are *c*-axis oriented and fabricated by co-evaporation of Y, Cu, and $BaF_2$ on $LaAlO_3$ substrates, followed by *ex situ* annealing.[8] The thickness of the films varies from 10 to 200 nm. The 50-, 100-, and 200-nm films are prepared by a two-stage annealing process using flowing wet and dry oxygen gas in a tube furnace. These films are annealed at a maximum temperature of 900 °C for 30 min in wet $O_2$ and at 525 °C for 30 min in flowing dry $O_2$. The first-stage annealing conditions for the 10- and 25-nm films are 750 °C for 30 min using a $N_2$:$O_2$ gas mixture (1% $O_2$) bubbled through deionized water. Normal (SEM) and high-resolution (HRSEM) scanning electron microscopy, Rutherford backscattering spectrometry (RBS), and x-ray diffraction measurements have been performed on samples from the same batches. The electrical resistivity at temperatures from $T_c$ to room temperature is measured by soldering four gold leads with indium to a sample surface in the van der Pauw arrangement. The 50-, 100-, and 200-nm films are *c*-axis oriented and possess high structural and morphological quality.[8,9] The crystalline structure of the 25-nm film is close to that of the thick films, while the crystalline structure of the 10-nm film is not as good as that of the others. Because the surface roughness is of the order of film thickness, the 10-nm film possesses island structures and the dc electrical resistivity

 

of this film is large compared with that of the other films. The substrate thicknesses are approximately 0.5 mm.

A Biorad FTS-60A Fourier-transform infrared spectrometer is employed to measure the reflectance of the film-substrate composites for the spectral region between 100 and 10000 $cm^{-1}$ at 300, 78, and 10 K. The reflectance is measured at approximately a 10° angle of incidence. The measurement technique was described in detail by Zhang *et al.*[7]

Electron motion in the *a-b* plane of $YBa_2Cu_3O_7$ superconductors above its critical temperature of about 90 K resembles that in a normal metal. The electron scattering rate is determined at 300 K by fitting the Drude model to the measured near-normal reflectance. In the superconducting state, the scattering rate of each film is determined at 10 and 78 K by fitting the infrared spectroscopic data using the algorithm developed by Zimmermann *et al.*[10] for the frequency-dependent electrical conductivity of superconductors with arbitrary purity. A temperature-independent fraction of residual normal-state electrons is included at temperatures below $T_c$. The scattering rate is also determined from kinetic theory using an extrapolation of the electrical resistivity to low temperatures based on Matthiessen's rule and the Bloch theory for the phonon-limited resistivity.

## II. ELECTRICAL RESISTIVITY

Kinetic theory relates the electron scattering rate $1/\tau$ to the dc electrical resistivity $\rho$ by

$$\frac{1}{\tau}=\rho\frac{n e^2}{m^*} , \tag{1}$$

where $e$ is the electron charge, $m^*$ the electron effective mass, and $n$ the electron number density. Fiory *et al.*[11] determined $m^*$ and $n$ for transport in the *a-b* plane of $YBa_2Cu_3O_7$ from measurements of the influence of charge-density modulation on the sheet inductance and sheet resistance of epitaxial $YBa_2Cu_3O_7$ films. The value of $m^*=4.3\times10^{-30}$ kg reported for the sample with the lowest normal-state electrical resistivity is employed in the present analysis. These authors found that the electron number density is independent of temperature in both the superconducting and normal states but varies among samples. In the present analysis, the electron number density is obtained for each film from Eq. (1) using the optically determined dc electrical resistivity, which is in good agreement with that from transport measurements, and electron scattering rate at room temperature. The method to determine the optical dc electrical resistivity is discussed in Sec. III A.

The normal-state dc electrical resistivity is extrapolated to temperatures below $T_c$ using Matthiessen's rule,[12]

$$\rho(T)=\rho_d+\rho_s(T) , \tag{2}$$

where $\rho_d$ is the electrical resistivity due to defects, which is independent of temperature, and $\rho_s$ is the electrical resistivity resulting from scattering by phonons. The Bloch formula yields $\rho_s$ in a normal metal,[12]

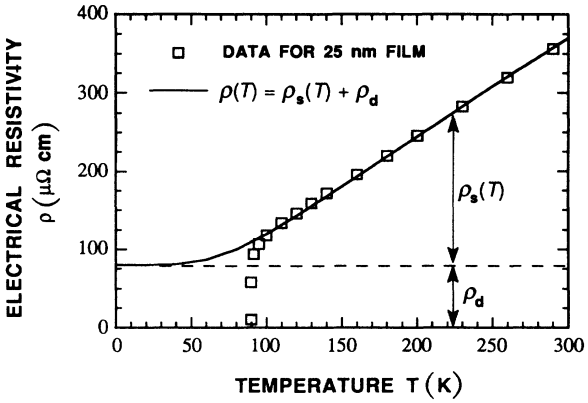


FIG. 1. Comparison of the fitted electrical resistivity with the measured data for the 25-nm *c*-axis-oriented $YBa_2Cu_3O_7$ film.

$$\rho_s(T)=4\,\rho_\Theta\left[\frac{T}{\Theta}\right]^5\int_0^{\frac{\Theta}{T}}\frac{x^5e^x}{(e^x-1)^2}dx , \tag{3}$$

where $\Theta$ is the Debye temperature and $\rho_\Theta$ is a constant. Goodson and Flik[3] estimated the Debye temperature in $YBa_2Cu_3O_7$ to be 470 K from the specific-heat data measured by Lang *et al.*[13] at 90 K. The dc electrical resistivity is fitted to experimental electrical resistivity data above $T_c$ using $\rho_d$ and $\rho_\Theta$ as adjustable parameters, providing the hypothetical electrical resistivity below the critical temperature if the material were in the normal state. After the electrical resistivity is obtained, Eq. (1) is employed to determine the electron scattering rate using the temperature-independent electron number density.

Figure 1 illustrates the application of the fitting technique to the resistivity of one of the films used in the present study. The solid line is the sum of the phonon and defect components of the electrical resistivity given by Eq. (2). The dashed line is the temperature-independent defect component of the total resistivity.

## III. INFRARED SPECTROSCOPY

Since the radiation penetration depth is larger than the film thickness, the optical properties of the $LaAlO_3$ substrate must be considered. Choi *et al.*[14] and Zhang *et al.*[7] measured the transmittance and reflectance of a 446-$\mu$m-thick $LaAlO_3$ substrate at 300, 78, and 10 K in the spectral region from 100 to 10000 $cm^{-1}$. They extracted the optical constants of the $LaAlO_3$ substrate from the reflectance and transmittance in the region from 1000 to 10000 $cm^{-1}$, where the substrate is partially transparent, and from the reflectance using the Kramers-Kronig relations for frequencies from 100 to 1000 $cm^{-1}$, where the substrate is opaque. Three peaks were observed in the reflectance spectra of $LaAlO_3$ due to phonon oscillators.

The frequency-dependent dielectric function of the $YBa_2Cu_3O_7$ films can be expressed as a linear superposition[10,15]

$$\epsilon(\omega)=\epsilon_\infty+\epsilon_{\text{phonon}}+\frac{\omega_{pe}^2}{\omega_e^2-\omega^2-i\omega\gamma_e}+\frac{i\sigma(\omega)}{\omega\epsilon_0} . \tag{4}$$

The first term on the right, $\epsilon_\infty$, is the high-frequency dielectric constant, which is approximately 4.[15] The second term is the phonon contribution. The third term is due to a temperature-independent mid-infrared band, which has a center frequency of $\omega_e$, a plasma frequency of $\omega_{pe}$, and a width of $\gamma_e$. The last term is the contribution of free carriers, where $\epsilon_0$ is the electrical permittivity of free space and $\sigma(\omega)$ is the free-carrier conductivity.

The contribution of phonons to the *a-b* plane dielectric function of $YBa_2Cu_3O_7$ is neglected in the present study due to their weak oscillator strengths.[16] The parameters for the mid-infrared band are taken from the data of Bauer[17] for the electric vector perpendicular to the *c* axis: $\omega_e = 1800\ \text{cm}^{-1}$, $\omega_{pe} = 24\,150\ \text{cm}^{-1}$, and $\gamma_e = 7500\ \text{cm}^{-1}$.

### A. Free-carrier conductivity in the normal state

At temperatures above the critical temperature, the free-carrier conductivity can be expressed as a function of frequency using the Drude model,

$$\sigma_n(\omega) = \frac{\sigma_{\text{dc}}}{1 - i\omega\tau}\ , \tag{5}$$

where $\tau$ is the relaxation time and its inverse is the scattering rate, $\sigma_{\text{dc}}$ is the dc electrical conductivity, and its inverse, $\rho_{\text{ir}}$, is the optical dc electrical resistivity.

Based on thin-film optics, the reflectance can be determined from the optical constants and the thicknesses of the film and substrate.[14] From 100 to 1000 $\text{cm}^{-1}$, where the substrate is opaque, the expression for the reflectance of the film-substrate composite is identical to that derived by Born and Wolf[18] for an absorbing film adjacent to an absorbing semi-infinite medium. Thin-film optics for a two-layer system is applied for a frequency region from 1000 to 10 000 $\text{cm}^{-1}$ by assuming that the electromagnetic wave is totally coherent in the film and totally incoherent in the substrate. By comparing the calculated reflectance with the measured data, the best fitting parameters are obtained, yielding the optical dc electrical resistivity and electron scattering rate at room temperature.

Figure 2 shows the calculated and measured reflectance at room temperature. For the 100-nm film, the calculated reflectance is very close to the measured data. The peaks at 190, 430, and 650 $\text{cm}^{-1}$ in the reflectance are due to the substrate, since the $YBa_2Cu_3O_7$ films are not opaque. The mid-infrared band introduces a broadband absorption around the center frequency of 1800 $\text{cm}^{-1}$, but does not cause a peak in the reflectance since its contribution to the dielectric function is much less than that of the free-carrier conductivity for frequencies less than $\omega_e$. The fitting parameters for each sample are listed in Table I. The electron number density is calculated from Eq. (1) using the values of $\rho_{\text{ir}}$ and $1/\tau$. The root-mean-square deviation between the calculated reflectance and the measured data is less than 3%. The photometric accuracy is estimated to be better than 3% for room-temperature reflectance measurements.[7]

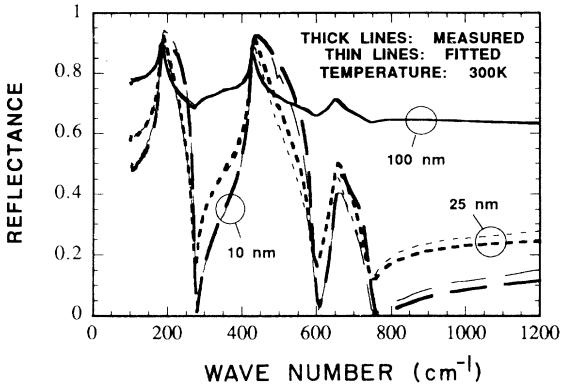


FIG. 2. Comparison of the calculated and measured reflectance at 300 K.

### B. Free-carrier conductivity at temperatures below $T_c$

The theory of Zimmermann *et al.*[10] is employed to calculate the frequency-dependent complex conductivity $\sigma_{ss}$ for BCS electrons, i.e., the electrons whose behavior can be modeled by the BCS theory.[19] This theory was developed by Lee *et al.*[20,21] from a quasiclassical linear-response model, in which the free-carrier excitations are modeled as quasiparticles. They solved the dynamical equations formulated using energy-integrated Green's functions by modeling the response of quasiparticles to a time- and space-dependent perturbation. The theory applies to weak-coupling isotropic BCS superconductors and is valid for any value of the electron scattering rate. The input parameters are the ratio of the temperature at which the samples are investigated to the critical temperature, $T/T_c$, the dc conductivity $\sigma_{\text{dc}}$, and a normalized

TABLE I. Fitting parameters and scattering rates obtained from infrared spectroscopy of $YBa_2Cu_3O_7$ *c*-axis films, electric vector in the *a-b* plane.

| | | $T=300$ K | | | $T=78$ K | | $T=10$ K | |
|---|---|---|---|---|---|---|---|---|
| $d_F$ (nm) | $T_c$ (K) | $\rho_{\text{ir}}$ ($\mu\Omega$ cm) | $1/\tau$ ($\text{cm}^{-1}$) | $n$ ($\text{m}^{-3}$) | $Y$ | $1/\tau$ ($\text{cm}^{-1}$) | $Y$ | $1/\tau$ ($\text{cm}^{-1}$) |
| 10 | 85 | 880±220 | 300±90 | $1.1\times10^{27}$ | 1.60±0.60 | 161±60 | 0.60±0.20 | 130±45 |
| 25 | 90 | 420±40 | 400±60 | $3.0\times10^{27}$ | 0.95±0.15 | 125±20 | 0.42±0.05 | 91±11 |
| 50 | 89 | 340±30 | 520±50 | $4.8\times10^{27}$ | 1.02±0.10 | 129±13 | 0.44±0.04 | 95±9 |
| 100 | 91 | 340±30 | 480±50 | $4.5\times10^{27}$ | 0.94±0.10 | 129±14 | 0.42±0.04 | 91±9 |
| 200 | 91 | 510±30 | 500±50 | $3.1\times10^{27}$ | 0.90±0.10 | 124±14 | 0.46±0.04 | 100±9 |

scattering rate

$$Y=h/(4\pi\tau\Delta) , \tag{6}$$

where $h$ is Planck's constant and $\Delta$ is the energy gap. The energy gap is related to temperature by an approximation to the BCS theory:[19,22]

$$\frac{\Delta(T)}{\Delta_0}=\left[1-\frac{T}{T_c}\right]^{1/2}\left[0.9663+0.7733\frac{T}{T_c}\right] \quad \text{for } \frac{T}{T_c}>0.3$$

and (7)

$$\Delta(T)/\Delta_0=1 \quad \text{for } T/T_c\leq 0.3 .$$

The BCS value of the energy gap at zero temperature is $A=2\Delta_0/kT_c=3.53$ where $k$ is the Boltzmann constant. Recent infrared studies showed evidence of a relatively large normalized energy gap, $2\Delta_0/kT_c$, between 7 and 8.[23–25] The effect of the gap parameter on the calculated reflectance will be examined in Sec. IV B.

Noting that at zero temperature $Y=(\pi/2)(\xi/\Lambda)$, where $\xi$ is the superconductor coherence length and $\Lambda$ is the electron mean free path, the normalized scattering rate can be viewed as a measure of the purity of superconductors. The mean free path is related to the Fermi velocity $v_F$ and the scattering rate by $\Lambda=v_F\tau$, and at zero temperature, $\xi_0=hv_F/(2\pi^2\Delta_0)$. The Fermi velocity is related to the number density and the effective mass by[12]

$$v_F=\frac{h(3\pi^2 n)^{1/3}}{2\pi m^*} . \tag{8}$$

For $Y\gg 1$, when the superconductor is in the impure limit, the Zimmermann theory gives the same result as the Mattis-Bardeen relations.[26] In the impure limit, the electron mean free path is much shorter than the superconductor coherence length. For a pure superconductor with $Y<1$, which is the case for $YBa_2Cu_3O_7$, the error resulting from using the Mattis-Bardeen relations is large. The effect of the electron scattering rate on the frequency-dependent conductivity in the superconducting state was shown by Tinkham.[27] Similar expressions for the frequency-dependent complex conductivity of superconductors with arbitrary scattering rates were derived by Leplae[28] and applied by Rao *et al.*[29] to high-$T_c$ superconductors.

Recent far-infrared[30–34] and microwave[6,23,35–37] measurements of single-crystal and thin-film $YBa_2Cu_3O_7$ superconductors indicated a residual absorption at temperatures much less than $T_c$ due to the existence of nonpairing charge carriers. As suggested by Kobayashi and Imai,[36] a temperature-independent fraction of residual normal-state electrons is considered, which obeys the Drude model. A physical explanation for the residual normal-state electrons is given in Sec. IV D. The combined free-carrier conductivity at temperatures below $T_c$ is given by

$$\sigma_s(\omega)=(1-f_{nr})\sigma_{ss}(\omega)+f_{nr}\sigma_{nr}(\omega) , \tag{9}$$

where $f_{nr}$ is the fraction of residual normal-state electrons, $\sigma_{ss}$ is calculated from the Zimmermann theory, and $\sigma_{nr}$ from Eq. (5). Kobayashi and Imai[36] determined $\sigma_{ss}(\omega)$ in Eq. (9) with the two-fluid model.[15] With the additional temperature-independent fraction of residual normal-state electrons, they suggested a three-fluid model to obtain agreement with microwave surface resistance measurements. Van der Marel *et al.*[24,38] proposed an *ad hoc* two-fluid model. In this model, $\sigma_{ss}(\omega)$ is calculated from the Zimmermann theory using a temperature-independent energy gap, $(1-f_{nr})$ is proportional to $[1-(T/T_c)^4]$ below $T_c$, and $\sigma_{nr}(\omega)$ is calculated from a temperature- and frequency-dependent scattering rate. In the present analysis, $f_{nr}$ is assumed to be independent of temperature and a frequency-independent scattering rate is used for both the residual normal-state electrons and the BCS electrons. The dc electrical conductivity, $\sigma_{dc}$, for the evaluation of $\sigma_{ss}$ and $\sigma_{nr}$ at low temperatures is obtained from the extrapolated resistivity as described in Sec. II.

Another theory, the effective-medium theory, was often employed for the study of inhomogeneous superconductors and yields a similar weighted sum of the two components for the normal-state and BCS electrons. It was derived from the coherent-potential approximation[39] and applied to high-$T_c$ materials by Glass and Hall,[40] Walker and Scharnberg,[41] and Rao *et al.*[29] Since the mechanism of the electrodynamic response of high-$T_c$ materials is still not fully understood, Eq. (9) is employed in the present study because of its simplicity and clear physical interpretation.

The best-fitting values of $Y$ and $f_{nr}$ are determined for each sample by comparing the calculated reflectance with the measured data. Figures 3 and 4 show the calculated and measured reflectance at 78 and 10 K for different film thicknesses. The three peaks are due to the phonon oscillators of the substrate, as in the case with the room-temperature reflectance. The far-infrared measurements between 100 and 400 $cm^{-1}$ are performed using a room-temperature DTGS pyroelectric detector and a polyethylene window for the vacuum seal of the sample holder. Because of the low optical efficiency of the

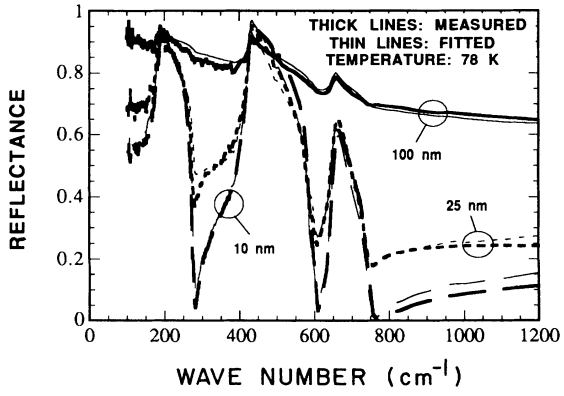


FIG. 3. Comparison of the calculated and measured reflectance at 78 K.

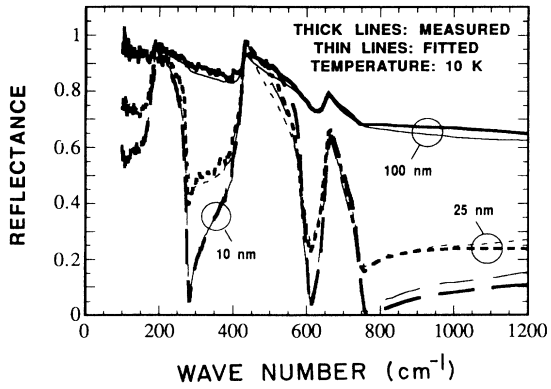


FIG. 4. Comparison of the calculated and measured reflectance at 10 K.

reflectance accessory for the low-temperature measurements, the optical signal that reaches the detector is much weaker than that for the room-temperature measurements, yielding a low signal-to-noise ratio in the far-infrared region. The fluctuation for the reflectance data at 10 and 78 K in the far-infrared region is due to the measurement uncertainty caused by the noise. At 10 and 78 K, the relative uncertainty is estimated to be 5% from 450 to 2000 $cm^{-1}$ and 10% from 100 to 450 $cm^{-1}$. The maximum deviation between the calculated and measured reflectance is 10%, and the standard deviation of these fittings is less than 4%. Note that the calculated reflectance is not sensitive to $f_{nr}$ for frequencies higher than the gap frequency of 217 $cm^{-1}$, and is not sensitive to the scattering rate for frequencies lower than 217 $cm^{-1}$. The value of $f_{nr}$ obtained for all samples is 0.5 with an uncertainty of $\pm 0.2$, due to the uncertainty in the measured far-infrared reflectance. The uncertainty of $f_{nr}$ does not affect the electron scattering rate obtained from this study, because $f_{nr}$ only influences the calculated reflectance for frequencies below 217 $cm^{-1}$.

## IV. DISCUSSION

### A. Electron scattering rate

Table I lists the optically obtained scattering rate for each film at 10, 78, and 300 K. The uncertainty of the scattering rate is based on the fitting in the spectral region of 217 to 1200 $cm^{-1}$, since the data in this region are more sensitive to the scattering rate. The uncertainty of the optical dc resistivity at room temperature is based on the fitting for the frequency region from 100 to 10 000 $cm^{-1}$. The electron number density is calculated from Eq. (1) using the optical dc electrical resistivity $\rho_{ir}$ and the electron scattering rate obtained at room temperature. At room temperature, the 10- and 25-nm films possess the lowest scattering rates. At low temperatures, the scattering rates for all films are very close except that of the 10-nm film. The electrical resistivities and the electron scattering rates calculated from Eq. (1) are listed in Table II. The uncertainty of each electrical resistivity and electron scattering rate given in Table II is 10%. The fitted optical dc electrical resistivity $\rho_{ir}$ at room temperature agrees with the value of $\rho$ obtained through transport measurements within the uncertainties of the fitting technique and the measured resistivity. The electrical transport resistivities $\rho$ at 10 and 78 K are extrapolated from the normal-state electrical resistivity data using Eqs. (2) and (3). The scattering rates for films of thickness from 25 to 200 nm are close at low temperatures. Tables I and II show that, except for the 10-nm film, the optically obtained scattering rate is in good agreement with that obtained from transport electrical resistivity data. An average scattering rate of 91 $cm^{-1}$ is determined at 10 K from both methods for films from 25 to 200 nm. The electron mean free path for these films at 10 K is $\Lambda = v_F \tau \sim 7$ nm.

For the 10-nm film, the optically obtained scattering rate is 40% larger than the average value for the other films, while that obtained from the electrical resistivity measurement is about 40% less than the average value for the other films. This may be due either to boundary scattering or to the differences in the crystalline structure between the 10-nm films and the other films. Because the electron mean free path is of the order of the film thickness, boundary scattering is important in this case, which causes an increase in the scattering rate. The electrical resistivity data employed in the extrapolation given by Eqs. (2) and (3) are fitted to data at temperatures above the critical temperature where the electron mean free path is about half as long.[3] Therefore, boundary scattering is not fully accounted for in the calculation of the scattering rate from the electrical resistivity, yielding an underprediction of the scattering rate. The reflectance of the film-substrate composite for the 10-nm film is very close to that of the bare substrate, which makes it

TABLE II. Scattering rates calculated from the electrical resistivity obtained through transport measurements in the *a-b* plane of $YBa_2Cu_3O_7$ films. An uncertainty of 10% applies to the electrical resistivity and the scattering rate.

| | $T=300$ K | | $T=78$ K | | $T=10$ K | |
|---|---|---|---|---|---|---|
| $d_F$ (nm) | $\rho$ ($\mu\Omega$ cm) | $1/\tau$ ($cm^{-1}$) | $\rho$ ($\mu\Omega$ cm) | $1/\tau$ ($cm^{-1}$) | $\rho$ ($\mu\Omega$ cm) | $1/\tau$ ($cm^{-1}$) |
| 10 | 840 | 286 | 210 | 72 | 160 | 55 |
| 25 | 360 | 343 | 105 | 100 | 80 | 76 |
| 50 | 295 | 451 | 80 | 122 | 60 | 92 |
| 100 | 330 | 466 | 85 | 120 | 65 | 92 |
| 200 | 520 | 510 | 120 | 118 | 90 | 88 |

difficult to extract accurately the scattering rates and the optical dc electrical resistivity from the fitting method. The uncertainty of the fitting parameters for this film is about 30% as listed in Table I. This uncertainty affects the optically obtained scattering rate and the electron number density, a parameter used to calculate the scattering rate from the electrical resistivity. The difference between the crystalline structure of the 10-nm film and that of the other films may also cause a disagreement in the electron scattering rates. Due to the island structure of the 10-nm films, the application of thin-film optics to these films could introduce an additional uncertainty in the spectroscopic method.

The electron scattering rates obtained in this study at 78 K for films of thickness from 25 to 200 nm are between 100 and 130 $cm^{-1}$, which are in agreement with the values between 100 and 110 $cm^{-1}$ obtained by Kamaras *et al.*[2] for different $YBa_2Cu_3O_7$ films at 100 K. The scattering rate of $YBa_2Cu_3O_7$ crystals obtained at 100 K by Orenstein *et al.*[5] from infrared spectroscopy is 140 $cm^{-1}$. The electron mean free path of 7 nm at 10 K determined in the present study for films of thickness from 25 to 200 nm is in good agreement with the value of 6 nm obtained by Goodson and Flik[3] for an $YBa_2Cu_3O_7$ single crystal using the electrical resistivity data. The average value of the normalized scattering rate $Y$ at 10 K for films of thickness from 25 to 200 nm is 0.42, which is less but not much less than unity. The superconductor $YBa_2Cu_3O_7$ is pure, but not in the extreme pure limit. The average carrier number density obtained in this study for film thickness from 25 to 200 nm is $3.9\times10^{27}$ $m^{-3}$, in good agreement with the average value of $4.9\times10^{27}$ $m^{-3}$ determined by Fiory *et al.*[11] for six epitaxial $YBa_2Cu_3O_7$ films from transport measurements.

A frequency-independent electron mass and scattering rate are successfully applied in the present study for frequencies below 1200 $cm^{-1}$, together with a mid-infrared absorption band. A frequency-dependent electron mass and scattering rate are often employed when analyzing the spectra of $YBa_2Cu_3O_7$ superconductors in the normal state, as proposed by Schlesinger *et al.*,[25] Schützmann *et al.*,[42] and Renk *et al.*[16] In these studies, the scattering rate changed almost linearly with frequency for frequencies below 2000 $cm^{-1}$.

Hylton and Beasley[1] estimated a minimum defect density in the *a-b* plane of $N=3.5\times10^{16}$ $m^{-2}$ to account for the critical current density measured along that plane. Neglecting electron motion normal to the *a-b* plane, the interacting range of the defects, $L$, can be related to the electron mean free path and the defect density per unit area, $N$, by $L=(\Lambda N)^{-1}$. Based on this relation, an average defect interaction range in the *a-b* plane of $L=4$ nm is obtained. It must be investigated whether this interaction range is compatible with the postulated nature of the defects, i.e., oxygen or cation point defects.

Siegal *et al.*[9] employed SEM, HRSEM, and RBS to investigate the microstructure of $YBa_2Cu_3O_7$ films, which were deposited by the same procedure as that of the 50-, 100-, and 200-nm films used in this study. Several types of defects existed in the films, such as pinholes and microcracks. These pinholes were normally less than 50 nm in size and occurred at a density of $10^{13}$ $m^{-2}$. Small structural imperfections due to edge dislocations, twin boundaries, and point defects are not detectable by these methods. Recently, scanning tunneling microscopy and atomic force microscopy were employed by Hawley *et al.*[43] and Gerber *et al.*[44] to observe screw dislocations in epitaxial $YBa_2Cu_3O_7$ films grown by magnetron sputtering. These studies revealed a spiral growth mechanism and provided hypotheses for the cause of the high critical current density in the films based on the observed defect densities of the order of $10^{13}$ $m^{-2}$.

### B. Influence of the energy gap parameter

The issues regarding the value and even the existence of the energy gap have not been resolved. Recent infrared studies show strong evidence for the existence of an energy gap between 400 and 500 $cm^{-1}$ ($2\Delta_0/kT_c\sim7-8$) for $YBa_2Cu_3O_7$ superconductors.[23–25] Hirata and Asada[45] reviewed the energy gap reported from far-infrared, Raman-scattering, and tunneling measurements, and concluded that the size of the energy gap of superconducting oxides is in agreement with the weak-coupling BCS prediction. Park and Chang[46] investigated the effect of the electronic pairing mechanism on the energy gap for high-$T_c$ superconducting oxides. They found a BCS gap $2\Delta_0/kT_c\sim3.56-4.02$ for both La- and Y-based systems and suggested that a large gap resulted from a low-energy excitation that may be phononic in origin. The effect of the energy gap on the predicted reflectance is investigated in the present work by varying the gap parameter $A$ from 3.53 to 8. The best fitting is always obtained by using the same scattering rate $1/\tau$ as listed in Table I. It follows that the electron scattering rate determined from this study is not affected by the selection of the energy gap. Figure 5 shows the fitting at 10 K for the 100-nm films using different gap parameters. The scattering rate is fixed to $1/\tau=91$ $cm^{-1}$, and the fraction of the residual normal-state electrons is $f_{nr}=0.5$. The reflectance is not very sensitive to the energy gap. Therefore, the energy gap cannot be determined from this study.

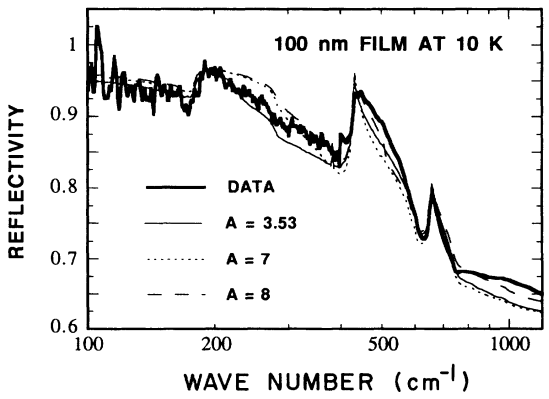


FIG. 5. The influence of energy gap on the predicted infrared reflectance at 10 K.

### C. Dynamical conductivity

The dynamical conductivity is related to the dielectric function obtained from Eq. (4) by[47]

$$\sigma_1(\omega)+\sigma_2(\omega)=-i\omega\epsilon_0\epsilon(\omega)\ . \tag{10}$$

Renk *et al.*[23] extracted the dynamical conductivity at 10 K for a 400-nm film from the infrared reflectivity and microwave surface resistance measurements by employing the Kramers-Kronig relations. The $YBa_2Cu_3O_7$ film was deposited *in situ* on a $SrTiO_3$ substrate by laser ablation, yielding a highly *c*-axis-oriented epitaxial film with $T_c=91$ K. The dc conductivity extrapolated to 10 K was $2.5\times10^6\ \Omega^{-1}\,m^{-1}$. The dynamical conductivity for this sample is calculated here using the model for the free-carrier conductivity described in Sec. III B. Figure 6 shows a comparison of the calculated dynamical conductivity with that extracted by Renk *et al.*[23] In the calculation, the energy gap parameter is $A=8$, the fraction of the normal-state electrons is $f_{nr}=0.2$, and the normalized scattering rate is $Y=0.20$, yielding a scattering rate of $1/\tau=100\ cm^{-1}$. The modeled dynamical conductivity agrees well with that extracted, particularly considering the error in the Kramers-Kronig analysis caused by the uncertainty of the assumed frequency-dependent absorption in the very-low-frequency region. The electron scattering rate is in agreement with the average obtained for films of thickness from 25 to 200 nm.

Figures 7(a) and 7(b) present the real and imaginary dynamical conductivity calculated for the 100-nm film used in this study at 10, 78, and 300 K. The dynamical conductivity at 10 K calculated from the Mattis-Bardeen relations[26] without considering the contribution of residual normal-state electrons is also presented for comparison. The Mattis-Bardeen relations, valid only in the extreme impure limit, are not applicable to $YBa_2Cu_3O_7$. The dynamical conductivity obtained for film thickness from 25 to 200 nm is very close. The shift of the gap from approximately 217 $cm^{-1}$ at 10 K to approximately 133 $cm^{-1}$ at 78 K is determined by Eq. (7). If the residual normal-state electrons were not included, $\sigma_1$ at 10 K would approach zero toward zero frequency.

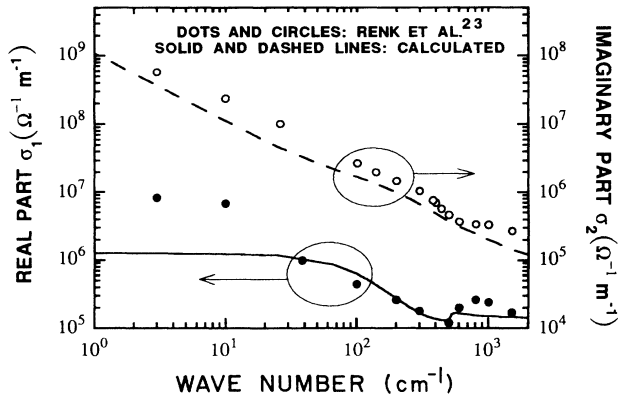


FIG. 6. Comparison of the calculated dynamical conductivity with that extracted from Kramers-Kronig analysis by Renk *et al.* (Ref. 23).

### D. Residual normal-state electrons

Microwave surface impedance and far-infrared absorption measurements provided evidence for nonpairing charge carriers. The origin of the residual normal-state carriers is not understood. The crystal structure varies from tetragonal for $YBa_2Cu_3O_6$, which is an insulator, to orthorhombic for the superconductor $YBa_2Cu_3O_7$. Van der Marel *et al.*[24] postulated the existence of a metallic nonsuperconducting phase in near-stoichiometric $YBa_2Cu_3O_7$ that does not change the lattice structure. Renk *et al.*[23,47] suggested that the residual absorption may not be of intrinsic nature but rather due to intergrain or impurity-induced absorption in defect regions of the film. Pham *et al.*[30] proposed a thin normal-conducting layer near the surface due to oxygen depletion. The reflectivity and absorptivity of untwinned single crystals with the electric vector polarized parallel to the *a* and *b* axes were measured by Schlesinger *et al.*,[34] Schützmann *et al.*,[48] and Pham *et al.*[30] The reflectivity for *a*-axis polarization was larger than that for *b*-axis polarization in the far-infrared region. The chain and plane contributions to the infrared conductivity were distinguished by those studies. By assuming that the conductivity of *a*-axis polarization results only from the $CuO_2$ planes, while that of *b*-axis polarization from both the $CuO_2$ planes and CuO chains, Schlesinger *et al.*[34] were able to associate 50–60 % of the infrared conduc-

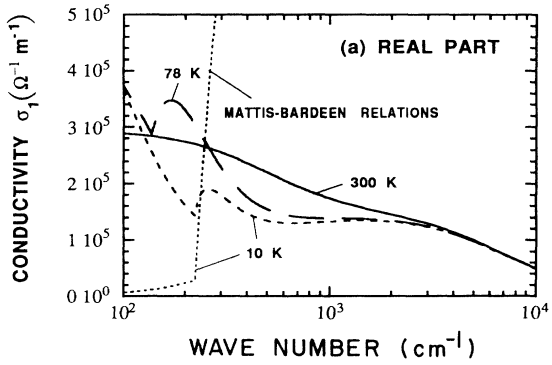


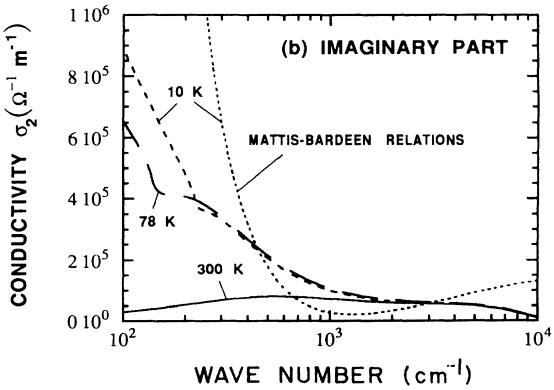


FIG. 7. Dynamical conductivity obtained at 300, 78, and 10 K for the 100-nm film.

tivity of *b*-axis polarization with the chains, suggesting that half of the free carriers are in the chains.

Choi *et al.*[14] investigated the effect of oxygen content on the optical constants of $YBa_2Cu_3O_{7-\delta}$ films and obtained a correlation between the oxygen content and the free-carrier number density. When the oxygen stoichiometry varies from 7 to 6.8, i.e., $\delta$ from 0 to 0.2, the free-carrier number density is reduced by a factor of 5. This was explained by a charge-transfer picture proposed by Cava *et al.*[49,50] In this model, the CuO chains serve as electron reservoirs, while the $CuO_2$ planes possess positive charges, i.e., holes. It is believed that the superconductivity of $YBa_2Cu_3O_7$ occurs in the $CuO_2$ planes, and that the material is a hole conductor. As oxygen atoms are removed from the CuO chains, some of the electrons that were originally attached to these oxygen atoms may either become free electrons in the CuO chains or transfer to the $CuO_2$ planes and neutralize the holes in the planes, resulting in an increase of the number of residual normal-state electrons in the CuO chains and a decrease of the hole population in the $CuO_2$ planes. The dimensions of a unit cell of $YBa_2Cu_3O_7$ are approximately $0.38\times0.39\times1.17$ nm$^3$.[49] If $\delta$ is changed from 0 to 0.05, a maximum of $5.8\times10^{26}$ m$^{-3}$ more free electrons can be released, which is about 10–20% of those obtained in the present study and by Fiory *et al.*[11] Cava *et al.*[49] determined a bond valence sum for the chain copper atoms of approximately 2.4 for $\delta\rightarrow0$, implying that the maximum possible number density of free electrons in the CuO chains is $2.3\times10^{27}$ m$^{-3}$. This is comparable with the total number density of the carriers in this material. In view of these results, the free carriers in the CuO chains could be the origin of the residual normal-electron absorption of the high-$T_c$ superconducting oxides. At temperatures below $T_c$, the carriers in the $CuO_2$ planes behave as BCS electrons and can be modeled using the theory of Zimmermann *et al.*,[10] while the conductivity of the free electrons in the CuO chains follows the Drude expression. In a fully oxidized $YBa_2Cu_3O_7$ superconductor, the number density of free carriers in the CuO chains has not been determined. More detailed investigation is required to establish a correlation among the oxygen deficiency $\delta$, the carrier densities in the CuO chains and in the $CuO_2$ planes, and the fraction of residual normal-state electrons.

## V. CONCLUSIONS

The electron scattering rate in the *a-b* plane of epitaxial $YBa_2Cu_3O_7$ films at temperatures well below $T_c$ found from infrared spectroscopy is in agreement with that determined using dc electrical resistivity data. A model for the free-carrier conductivity is developed using the theory of Zimmermann *et al.*[10] and a temperature-independent fraction of residual normal-state electrons. An average scattering rate of approximately 91 cm$^{-1}$ at 10 K is obtained for films of thickness from 25 to 200 nm, yielding an electron mean free path of 7 nm. Since the electron mean free path is comparable with the thickness of the 10-nm film, boundary scattering could increase the electron scattering rate in this very thin film. The deviation between the scattering rate of the 10-nm film and that of the other films may also be caused by the different microstructure of the 10-nm film. Although the superconductor $YBa_2Cu_3O_7$ is pure, i.e., $\xi/\Lambda\sim2/7<1$, it is not in the extreme pure limit of $\xi/\Lambda\ll1$. Using the defect density resulting from flux pinning considerations, an average defect interaction range of 4 nm is obtained.

## ACKNOWLEDGMENTS

This work was supported by the C. S. Draper Laboratory, Cambridge, MA, under Contract No. DL-H-418480, by the Lynde and Harry Bradley Foundation, and by the Alfred P. Sloan Foundation. K.E.G. acknowledges the support of the U.S. Office of Naval Research. Helpful discussions with Professor M. Tinkham and Professor T. P. Orlando are appreciated.

[1]T. L. Hylton and M. R. Beasley, Phys. Rev. B **41**, 11 669 (1990).
[2]K. Kamaras, S. L. Herr, C. D. Porter, N. Tache, D. B. Tanner, S. Etemad, T. Venkatesan, E. Chase, A. Inam, X. D. Wu, M. S. Hegde, and B. Dutta, Phys. Rev. Lett. **64**, 84 (1990).
[3]K. E. Goodson and M. I. Flik, J. Heat Transfer (to be published).
[4]J. L. Cohn, S. A. Wolf, T. A. Vanderah, V. Selvamanickam, and K. Salama, Physica C **192**, 435 (1992).
[5]J. Orenstein, G. A. Thomas, A. J. Millis, S. L. Cooper, D. H. Rapkine, T. Timusk, L. F. Scheemeyer, and J. V. Waszczak, Phys. Rev. B **42**, 6342 (1990).
[6]D. Miller, P. L. Richards, S. Etemad, A. Inam, T. Venkatesan, B. Dutta, X. D. Wu, C. B. Eom, T. H. Geballe, N. Newman, and B. F. Cole, Appl. Phys. Lett. **59**, 2326 (1991).
[7]Z. M. Zhang, B. I. Choi, T. A. Le, M. I. Flik, M. P. Siegal, and Julia M. Phillips, J. Heat Transfer (to be published).
[8]M. P. Siegal, Julia M. Phillips, R. B. van Dover, T. H. Tiefel, and J. H. Marshall, J. Appl. Phys. **68**, 6353 (1990).
[9]M. P. Siegal, Julia M. Phillips, A. F. Hebard, R. B. van Dover, R. C. Farrow, T. H. Tiefel, and J. H. Marshall, J. Appl. Phys. **70**, 4982 (1991).
[10]W. Zimmermann, E. H. Brandt, M. Bauer, E. Seider, and L. Genzel, Physica C **183**, 99 (1991).
[11]A. T. Fiory, A. F. Hebard, R. H. Eick, P. M. Mankiewich, R. E. Howard, and M. L. O'Malley, Phys. Rev. Lett. **65**, 3441 (1990).
[12]J. M. Ziman, *Electrons and Phonons* (Oxford University Press, Oxford, 1960).
[13]M. Lang, T. Lechner, S. Riegel, F. Steglich, G. Weber, T. J. Kim, B. Lüthi, B. Wolf, H. Rietschel, and M. Wilhelm, Z. Phys. B **69**, 459 (1988).
[14]B. I. Choi, Z. M. Zhang, M. I. Flik, and T. Siegrist, J. Heat Transfer (to be published).
[15]T. Timusk and D. B. Tanner, in *Physical Properties of High-Temperature Superconductors I,* edited by D. M. Ginsberg (World Scientific, Singapore, 1989), p. 339.

[16]K. F. Renk, H. Eschrig, U. Hofmann, J. Keller, J. Schützmann, and W. Ose, Physica C **165**, 1 (1990).
[17]M. Bauer, Ph.D. dissertation, Tübingen University, Germany, 1990 (unpublished).
[18]M. Born and E. Wolf, *Principles of Optics* (Pergamon, Oxford, 1980).
[19]J. Bardeen, L. N. Cooper, and J. R. Schrieffer, Phys. Rev. **108**, 1175 (1957).
[20]W. Lee, D. Rainer, and W. Zimmermann, Physica C **159**, 535 (1989).
[21]W. Lee, D. Rainer, and W. Zimmermann (unpublished).
[22]D. C. Carless, H. E. Hall, and J. R. Hook, J. Low Temp. Phys. **50**, 605 (1983).
[23]K. F. Renk, B. Gorshunov, J. Schützmann, A. Prückl, B. Brunner, J. Betz, S. Orbach, N. Klein, G. Müller, and H. Piel, Europhys. Lett. **15**, 661 (1991).
[24]D. van der Marel, H.-U. Habermeier, D. Heitmann, W. König, and A. Wittlin, Physica C **176**, 1 (1991).
[25]Z. Schlesinger, R. T. Collins, F. Holtzberg, C. Feild, G. Koren, and A. Gupta, Phys. Rev. B **41**, 11 237 (1990).
[26]D. C. Mattis and J. Bardeen, Phys. Rev. **111**, 412 (1958).
[27]M. Tinkham, in *Far-Infrared Properties of Solids,* edited by S. S. Mitra and S. Nudelman (Plenum, New York, 1970), p. 223.
[28]L. Leplae, Phys. Rev. B **27**, 1911 (1983).
[29]A. M. Rao, P. C. Eklund, G. W. Lehman, D. W. Face, G. L. Doll, G. Dresselhaus, and M. S. Dresselhaus, Phys. Rev. B **42**, 193 (1990).
[30]T. Pham, M. W. Lee, H. D. Drew, U. Welp, and Y. Fang, Phys. Rev. B **44**, 5377 (1991).
[31]E. Kawate, A. Onae, K. Isida, T. Tamegai, Y. Miki, and M. Okaji, Phys. Rev. B **43**, 12 976 (1991).
[32]F. Gao, G. L. Carr, C. D. Porter, D. B. Tanner, S. Etemad, T. Venkatesan, A. Inam, B. Dutta, X. D. Wu, G. P. Williams, and C. J. Hirschmugl, Phys. Rev. B **43**, 10 383 (1991).
[33]R. C. Budhani, L. Lesyna, D. DiMarzio, H. Wiesmann, and G. P. Williams, Phys. Rev. B **44**, 7087 (1991).
[34]Z. Schlesinger, R. T. Collins, F. Holtzberg, C. Feild, S. H. Blanton, U. Welp, G. W. Crabtree, Y. Fang, and J. Z. Liu, Phys. Rev. Lett. **65**, 801 (1990).
[35]G. Müller, N. Klein, A. Brust, H. Chaloupka, M. Hein, S. Orbach, H. Piel, and D. Reschke, J. Supercond. **3**, 235 (1990).
[36]Y. Kobayashi and T. Imai, IEICE Trans. E **74**, 1986 (1991).
[37]S. S. Laderman, R. C. Taber, R. D. Jacowitz, J. L. Moll, C. B. Eom, T. L. Hylton, A. F. Marshall, T. H. Geballe, and M. R. Beasley, Phys. Rev. B **43**, 2922 (1991).
[38]D. van der Marel, M. Bauer, E. H. Brandt, H.-U. Habermeier, D. Heitmann, W. König, and A. Wittlin, Phys. Rev. B **43**, 8606 (1991).
[39]G. L. Carr, S. Perkowitz, and D. B. Tanner, in *Infrared and Millimeter Waves,* edited by K. J. Button (Academic, Orlando, 1985), Vol. 13, p. 171.
[40]N. E. Glass and W. F. Hall, Phys. Rev. B **44**, 4495 (1991).
[41]D. Walker and K. Scharnberg, Phys. Rev. B **42**, 2211 (1990).
[42]J. Schützmann, W. Ose, J. Keller, K. F. Renk, B. Roas, L. Schultz, and G. Saemann-Ischenko, Europhys. Lett. **8**, 679 (1989).
[43]M. Hawley, I. D. Raistrick, J. G. Beery, and R. J. Houlton, Science **251**, 1587 (1991).
[44]C. Gerber, D. Anselmetti, J. G. Bednorz, J. Mannhart, and D. G. Schlom, Nature (London) **350**, 279 (1991).
[45]T. Hirata and Y. Asada, J. Supercond. **4**, 171 (1991).
[46]C. H. Park and K. J. Chang, Physica C **184**, 81 (1991).
[47]K. F. Renk, in *Studies of High Temperature Superconductors,* edited by A. V. Narlikar (Nova Science, New York, 1992), Vol. 10.
[48]J. Schützmann, B. Gorshunov, K. F. Renk, J. Münzel, A. Zibold, H. P. Geserich, A. Erb, and G. Müller-Vogt, Phys. Rev. B **46**, 512 (1992).
[49]R. J. Cava, A. W. Hewat, E. A. Hewat, B. Batlogg, M. Marezio, K. M. Rabe, J. J. Krajewski, W. F. Peck, Jr., and L. W. Rupp, Jr., Physica C **165**, 419 (1987).
[50]R. J. Cava, Science **247**, 656 (1990).